Photoinduced Aziridination Reaction Sensitized by PbO_x-Modified Zeolite

Fei-Ting Huang, Hsi-Jung Jao, Wei-Hsiu Hung,* Kwunmin Chen,* and Chong Mou Wang*

Department of Chemistry, National Taiwan Normal University, Taipei 116, Taiwan

Received: June 30, 2004; In Final Form: October 6, 2004

In this work, we report a photoinduced aziridination reaction sensitized by lead oxide-containing zeolite colloids ($NaY|PbO_x$). When *N*-aminophthalimide and 3-cinnamoyl-2-oxazolidinone were photolyzed with $NaY|PbO_x$, (2*R*,3*S*)- and (2*S*,3*R*)-*N*-phthalimidoaziridines were observed as the major products. Under similar conditions, bare zeolite Y showed an insignificant catalytic effect on this reaction. These results highlight that the contained PbO_x is a potential catalyst. According to X-ray photoelectron spectroscopy (XPS) and electrochemical characterizations, the contained lead oxide is firmly deposited on the host and behaves like an n-type semiconductor. The associated conduction band and valence-band edges are located at -0.5 ± 0.2 and 0.9 ± 0.2 V versus a saturated calomel electrode (SCE), respectively. Since the valence-band edge is positive enough to oxidize *N*-aminophthalimide, *N*-aminophthalimide radicals can be formed on the illuminated $NaY|PbO_x$ and react with 3-cinnamoyl-2-oxazolidinone to produce aziridine products. A 1-h irradiation provided the aziridine products in 3% yield and 93% selectivity. For the low yield, calculations based on the doping density of $NaY|PbO_x$ suggest that the penetration depth of light may not be sufficient to excite the majority carriers relative to the thickness of the space-charge layer. Due to this or another reason, such as light blocking by the metallic silver formed on the surface of $NaY|PbO_x$ when silver nitrate is used as the sacrificial acceptor, the efficiency in light harvesting may be limited in this case. Although limited by these drawbacks and the low concentration within NaY (<20 μg/g of NaY), the prepared $PbO_{x(NaY)}$ still behaves as an effective aziridination catalyst compared to some other photosensitizers. Noticeably, incorporating appropriate chiral ligands can advance the enantiomeric excess (ee) for the (2*S*,3*R*) isomer. X-ray absorption near-edge-structure (XANES) spectral measurements show that the incorporated chiral ligands may function as bidentate agents to interact with $PbO_{x(NaY)}$ and cause the binding energy of Pb (L_{III} edge) in $NaY|PbO_x$ to shift to a higher energy by $\sim$2.6 eV. Likely due to this chelating effect, an asymmetric oxidation of *N*-aminophthalimide results. A preferential formation for the (2*S*,3*R*) isomer becomes possible.

Introduction

The synthesis of functionalized, optically active molecules for stereoselective transformations is one of the ultimate challenges in chemistry. Many excellent approaches, such as asymmetric catalysis,[1] chiral ligand incorporation,[2] and aziridine mediation,[3] have been presented. Regarding the preparation of aziridine compounds, strategies based on transition-metal catalysis have shown promise.[4] In a recent study on alkene aziridination,[5] lead(IV) acetate was found to be a specific and effective oxidative catalyst and could be recoverable as lead oxide after use. Unfortunately, soluble lead species are not qualified green reagents from the aspect of green chemistry.[6] Large-amplitude controlled-potential electrolysis is thus considered to be an alternative and has shown promise in the preparation of aziridine compounds.[7] In fact, an approach based on photosensitization is also a potential alternative. In this work, we present such a possibility.

Photoinduced charge-transfer reactions are an ideal means for converting sunlight into electrochemical potential energy. Semiconductor-based[8] and multicomponent systems,[9] such as dyads and triads, that carry out a similar function may rival natural photosynthesis in terms of quantum yield, energy storage, and lifetime for charge separation. In many studies, aluminosilicates, like zeolites[10] and clays,[11] and many other solid phases, such as phosphates, γ-alumina, and silica gels,[12] have also proven to be useful hosts that can effectively compartmentalize the photocatalysts and products. Zeolites are microporous aluminosilicate materials made up of $[SiO_4]^{4-}$ and $[AlO_4]^{5-}$ tetrahedra arranged in a defined manner to give the material an open framework structure of cavities and pores. This property provides an opportunity to accommodate cationic or polar molecules within the cavities of zeolites.[13] Catalysts with a greater reaction cross section or surface area can thus be prepared.[14] Under a similar consideration, we have recently incorporated 9,10-dicyanoanthracene (DCA) and 9-cyanoanthracene (CA) within zeolite Y to elucidate the photosensitized oxygenation and fluorination reactions mediated by DCA and CA.[15] Semiconductor miniatures can also be encapsulated within zeolites. Semiconductor-incorporated zeolites have shown promise in photoinduced charge-transfer reactions[16] and many other applications such as chemical sensing.[17] In a recent study on the photoinduced charge-transfer reactions with semiconductor-incorporated zeolites, we found that lead oxide-containing zeolite Y (denoted $NaY|PbO_x$) functions as an n-type semiconductor. The valence-band edge is located near 0.9 V versus a saturated calomel electrode (SCE) in acetonitrile. Because this edge is positive enough to oxidize *N*-aminophthalimide, (2*R*,3*S*)- and (2*S*,3*R*)-*N*-phthalimidoaziridines can be produced from *N*-aminophthalimide and 3-cinnamoyl-2-oxazolidinone under the photosensitization with $NaY|PbO_x$. Although a 1-h photolysis provided these aziridine isomers in 3% yield, the selectively

10.1021/jp040462p CCC: $27.50
Published on Web 12/02/2004

was >93%. Several other semiconductors and photosensitizers were also tested for comparison. Equal-weighted TiO_2 (rutile and anatase) showed a greater catalytic impact on this reaction. However, greater amounts of side products were also produced in this case. CdS, CA, and $Ru(bpy)_3^{2+}$ that possess similar energetics of $NaY|PbO_x$ gave less significant catalytic impacts on the formation of aziridine products compared to $NaY|PbO_x$. Since the effective concentration of PbO_x in the zeolite was <20 μg/g of NaY, $NaY|PbO_x$ is highlighted as a specific aziridination catalyst. Noticeably, when $NaY|PbO_x$ is incorporated with appropriate camphor-derived chiral ligands, the (2*S*,3*R*) isomer can be produced with a greater yield, giving this isomer ~30% enantiomeric excess (ee). X-ray absorption spectroscopic analysis indicates that the L_{III} edge of Pb in $NaY|PbO_x$ shifts to a higher energy by ~2.6 eV after the incorporation of these chiral ligands. This result suggests that these chiral ligands may function as bidentate agents to interact with $PbO_{x(NaY)}$. Owing to this effect, the chirality of the adsorbed chiral ligand can manipulate the coordination geometry of $PbO_{x(NaY)}$. An asymmetric oxidation of *N*-aminophthalimide is thus allowed to take place on the surface of the excited $PbO_{x(NaY)}$. A preferential formation for the (2*S*,3*R*)-aziridine isomer thus results.

Experimental Section

N-Aminophthalimide, 3-cinnamoyl-2-oxazolidinone, and camphor-derived chiral ligands were synthesized according to the procedures reported previously.[5] Aziridination products were characterized on the basis of similar procedures reported in the literature.[5b] In principle, the (2*R*,3*S*) and (2*S*,3*R*) enantiomers were separated by high-performance liquid chromatography (HPLC) with a Chiralcel-AD chiral column. The absolute stereochemistry of the isomers was identified by chemical correlation with the established aziridines. The (2*R*,3*S*) enantiomer was treated with camphorpyrazolidinone in the presence of 4-(dimethylamino)pyridine (DMAP) to give the corresponding aziridine derivative. The absolute stereochemistry of the (2*R*,3*S*) isomer was then confirmed by the optical rotation ($[\alpha]_D$) analysis. Lead-exchanged zeolite particles ($NaY|Pb^{2+}$) were prepared by suspending 1 g of zeolite Y (in the Na form, Strem) in $Pb(NO_3)_2$ (1 mM, 0.5 L, TCI) for 48 h. After careful filtration and washing with water, the resulting powder was quenched by NaOH (1 M, Strem), followed by a calcination at 800 °C for 6 h. X-ray photoelectron spectroscopy (XPS) analysis showed that a certain portion of Pb^{2+} in the zeolite had been converted to PbO_x after heating. The loading of PbO_x in $NaY|PbO_x$ was estimated to be around 20 μg/g of NaY on the basis of the XPS peaks calibrated by equal-weighted zeolite mixed with varying amounts of polycrystalline PbO_x ($x \approx 2$, Aldrich).

The electrodes of $NaY|Pb^{2+}$ and $NaY|PbO_x$ were fabricated on conductive indium tin oxide (ITO) glass squares (indium-doped, 0.7 mm thick, 20 Ω/cm^2, Delta Technol.). Typically, a portion of zeolite slurry (30 μL cm^{-2}, 100 mg/100 mL water) was spin-coated onto the desired electrode and dried at room temperature. Unless otherwise mentioned, cyclic voltammograms (CVs) and linear-sweeping voltammograms (LSVs) were measured under nitrogen in a one-compartment cell using a standard three-electrode configuration. A saturated calomel electrode (SCE) was used as the reference electrode. For the systems in CH_3CN, a silver pseudoreference electrode was used instead. Potentials were calibrated against ferrocene ($E^{\circ\prime}$: 0.38 V vs SCE in $TBAClO_4/CH_3CN$). PAR 283 (EG&G Princeton Applied Research) and CV-50 (Bioanalytical System Inc.) instruments were used to measure the CV and LSV curves and for the electrolysis experiments. Mott−Schottky plots were carried out with a Voltalab 40 potentiostat (Radiometer, France). HPLC separation was performed with a system consisting of a gradient pump (Thermo Separation Products, P100), an injection valve (20-μL sample loop), and a Thermo Finnigan UV 6000 LP spectrophotometer detector. Diffuse-reflectance ultraviolet−visible (UV−vis) absorption spectra were recorded with a UV−vis spectrophotometer (JASCO model 7850). A high-pressure mercury lamp (1000 W, Oriel) with a 10-cm-long homemade water filter and desired band-pass filters (Toptical Scientific) was employed as the light source. ^1H NMR and ^{13}C NMR spectra were recorded at 400 MHz on a JEOL JNM EX400 spectrometer. The XPS and X-ray absorption near-edge-structure (XANES) measurements were conducted at the SRRC (Synchrotron Radiation Research Center, Taiwan). For XPS, the incident angle of photons was 55° from the surface normal. Emitted photoelectrons were collected with the electron analyzer normal to the sample surface in an angle-integrated mode. For the Pb L_{III}-edge XANES measurements, a 6-m high-energy spherical grating monochromator (HSGM) beamline was used.

Results and Discussion

Photosynthetic reaction centers are natural photovoltaics, which can convert sunlight into electrochemical potential energy. Many artificial systems based on semiconductor materials and multicomponent molecules have been investigated and shown to have potential in mimicking natural photosynthesis and many other applications.[18] Compared with TiO_2, MoO_3, or WO_3,[19−21] lead oxide (denoted PbO_x with $1 < x < 2$) seems to be less attractive in these aspects. According to our investigation, lead oxide is, in fact, a specific photocatalyst for alkene aziridination, such as the reaction between *N*-aminophthalimide and 3-cinnamoyl-2-oxazolidinone described in eq 1. This potential is

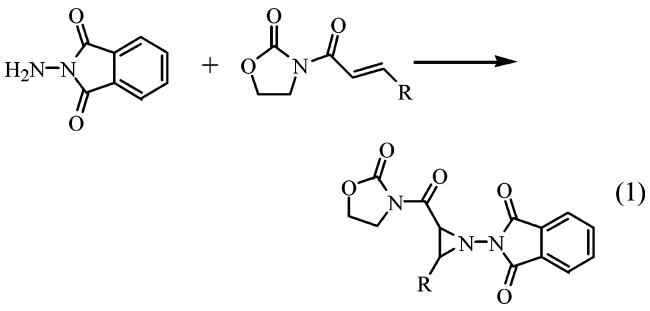

evidenced by the experimental results shown in Figure 1. When *N*-aminophthalimide (1 mmol) and equimolar 3-cinnamoyl-2-oxazolidinone were photolyzed with $NaY|PbO_x$ under the irradiation of white light, (2*R*,3*S*)- and (2*S*,3*R*)-*N*-phthalimidoaziridine isomers were observed as the major products (*m*/*e*, 377; retention time, 35.91 and 87.18 min, respectively). A 1-h photolysis provided these two aziridine isomers in 3% yield and 93% selectivity (equal amount, HPLC yield, relative to the internal standard: 3-cinnamoyl-2-oxazolidinone; enantiomeric excess determined by chiral HPLC analysis (Chiralcel AD)). Insignificant amounts of side products were observed in this case. ^1H NMR analysis agreed with the HPLC conclusion. Noticeably, when bare zeolite (equal weight) was used instead of $NaY|PbO_x$, negligible amounts of aziridination products were found. These results highlight that the PbO_x contained in the zeolite plays an essential role in reaction 1. To interpret this result, a reaction mechanism is proposed in Scheme 1, in which

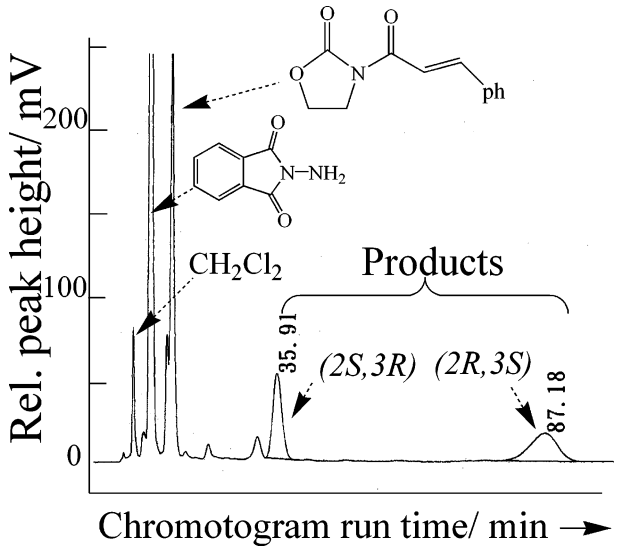

Figure 1. HPLC traces (monitored at 260 nm) recorded after the reaction of *N*-aminophthalimide with 3-cinnamoyl-2-oxazolidinone (1 mmol each in CH_3CN) under the sensitization with 40 mg of $PbO_{x(NaY)}$ and 2 equiv of $AgNO_3$ (N_2, white light, 1 h).

N-aminophthalimide (denoted imide) is oxidatively converted to the corresponding radical by the photoexcited NaY|PbO_x via two one-electron-transfer processes. The resulting radical is then coupled with 3-cinnamoyl-2-oxazolidinone (alkene) to give the (2*S*,3*R*)- and (2*R*,3*S*)-aziridine products.

$$PbO_{x(NaY)} + h\nu \rightarrow PbO_{x(NaY)}^* \quad (2)$$

$$PbO_{x(NaY)}^* \rightarrow PbO_{x(NaY)}(h^+ \text{--- } e^-) \quad (3)$$

$$PbO_{x(NaY)}(h^+ \text{ --- } e^-) + \text{imide} \rightarrow PbO_{x(NaY)}(e^-) + \text{imide}^+ \quad (4)$$

$$\text{imide}^+ + PbO_{x(NaY)}(h^+ \text{ --- } e^-) \rightarrow PbO_{x(NaY)}(e^-) + \text{radical} \quad (5)$$

$$\text{radical} + \text{alkene} \rightarrow \text{aziridine isomers} \quad (6)$$

$$2PbO_{x(NaY)}(e^-) + 2Ag^+_{(soln)} \rightarrow 2PbO_{x(NaY)} + 2Ag_{(s)} \quad (7)$$

To date, many approaches have been presented for the preparation of lead oxide and the associated modified electrodes.[22] To provide a greater cross section for bulk photolysis, we dispersed PbO_x on zeolite Y. The strategy was started from the preparation of NaY|Pb^{2+} and followed by a treatment with NaOH and calcination at 800 °C. Diffuse-reflectance absorption spectroscopic analysis showed that the absorbance of NaY|Pb^{2+} in the visible region (300−750 nm) increased significantly after calcination (Supporting Information Figure 1S). Lead oxide absorbs visible light (absorption edge ≈850 nm, $E_g \approx 1.4$ eV),[23] whereas Pb^{2+} ions absorb relatively weakly in the visible region. The rise in absorbance is thus attributed to the formation of PbO_x ($1 < x < 2$) on the zeolite. XPS measurements support this hypothesis. According to Figure 2A, the binding energies of Pb ($4f_{7/2}$ and $4f_{5/2}$) in NaY|Pb^{2+} are distributed around 127−145 eV. This distribution is similar to that found for $Pb(NO_3)_2$ (Supporting Information Figure 2S) except that the peaks in terms of the full widths at half-maximum (fwhm's) are relatively broader. From the broadened fwhm, we conclude that the adsorbed Pb^{2+} ions are randomly located over the surface or trapped in different sites of the zeolite. Both $Pb(NO_3)_2$ and NaY|Pb^{2+} show three major chemical states

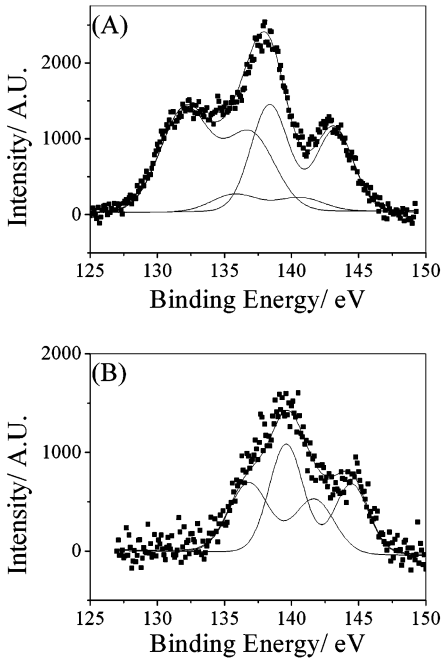

Figure 2. XPS spectra of NaY|Pb^{2+} before (A) and after (B) calcination (800 °C).

SCHEME 1: Schematic Illustration for the $PbO_{x(NaY)}$-Sensitized Aziridination Reaction

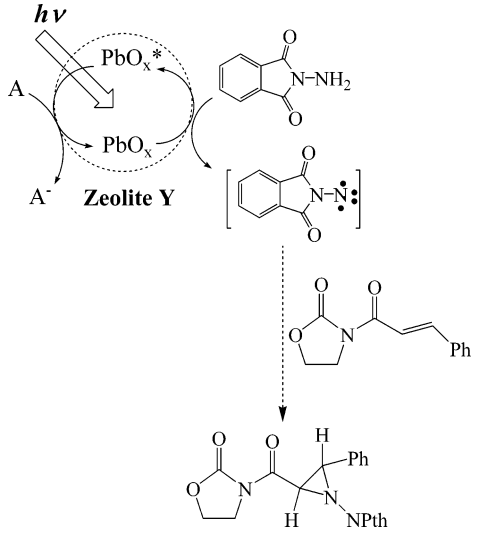

according to XPS (for each component, $\Delta = 4.8$ eV; integral peak area of $4f_{7/2}$ and $4f_{5/2}$ ≈8:6). There is a lack of evidence to identify these states. X-ray induction and/or impurity contamination are possible causes. Closer examinations of the XPS spectra of NaY|Pb^{2+} (Figure 2A) and NaY|PbO_x (Figure 2B) reveal that the Pb peaks in the lower-energy part (binding energies around 132−137 eV) diminish after heating. This spectral change matches well with the spectral difference between $Pb(NO_3)_2$ and PbO_x ($x \approx 2$, Supporting Information[24] Figure 3S), evidencing that a certain portion of Pb^{2+} in the zeolite has been successfully converted to the form of PbO_x after calcinations.

The contained lead oxide is electrochemically active, which is evidenced by the CV curves shown in Figure 3A recorded with a NaY|PbO_x-modified electrode in aqueous media. Comparisons of these waves with those recorded with the electrodes of NaY|Pb^{2+} (Figure 3B) and polycrystalline PbO_x (Figure 3C) suggest that the waves near −0.5 V correspond to $Pb^{II/0}$ and

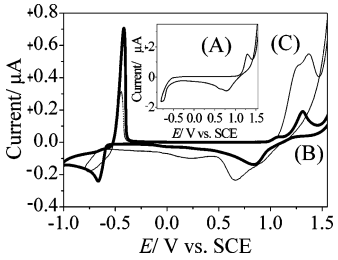

Figure 3. CV curves recorded with the electrodes of NaY|PbO_x (A), NaY|Pb^{2+} (B), and polycrystalline PbO_x (C) in 0.1 M KNO_3. Scan rate, 50 mV s^{-1}.

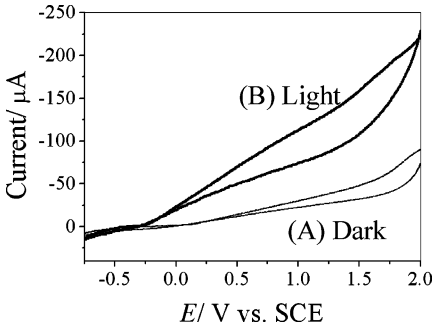

Figure 4. Typical CV curves recorded with the NaY|PbO_x electrode in CH_3CN|0.1 M $TBAClO_4$. Scan rate, 50 mV s^{-1}.

the other located near 1.0 V originated from $Pb^{II/IV}$.[25] In the case of NaY|PbO_x, the anodic lobe of the $Pb^{II/0}$ peak is missing. This phenomenon is tentatively attributed to the oxidation by the trapped oxygen or proton in the zeolite. Many other possibilities, such as reactive oxygen species formed in the lattices of $PbO_{x(NaY)}$ during catalyst preparation or potential scan, may also cause similar problems. Interstitial defects or oxide vacancies are likely to be created in NaY|PbO_x during preparation. The PbO_x species in the zeolite is thus expected to be an extrinsic material, which explains the conductivity revealed in the CV shown in Figure 3A. The waves depicted in Figure 3A show a negligible decay in current according to a long-term test by continuously cycling the electrode potential from −1.0 to 1.5 V. Leaching of Pb from the host is thus considered to be negligible. In contrast to the CV measured in aqueous KNO_3, the waves obtained in CH_3CN|0.1 M $TBAClO_4$ (Figure 4) are less prominent. In view of the fact that most hydrophilic metal oxides show poor affinity to hydrophobic solvents, we thus attribute this difference to an unfavorable solvation of lead species in CH_3CN. Nevertheless, the prepared PbO_x seems to retain its photoelectrochemical activity in this aprotic medium. When the electrode of NaY|PbO_x is irradiated with light, the anodic current is raised greatly. The onset potential is located at ∼ −0.3 V versus SCE. This electrochemical behavior agrees with that obtained with polycrystalline lead oxide.[26] According to the CV recorded between light and dark, the prepared $PbO_{x(NaY)}$ is considered to be an n-type semiconductor.[27] Mott−Schottky-plot analysis supports this conclusion.[28] The space-charge capacitance (C_{SC}) measured with a NaY|PbO_x electrode increases with a negative shift in E and has the following linear relationship:

$$C_{SC}^{-2} \approx (1.41 \times 10^{20}/N_D\epsilon)[E - E_{fb} - 0.026] \qquad (8)$$

Here, N_D and ϵ represent the doping density and dielectric constant of the prepared $PbO_{x(NaY)}$, respectively. From the intercept of the linear relationship between C_{SC}^{-2} and E plotted in Figure 5, the flatband potential (E_{fb}) of NaY|PbO_x is −0.5 ± 0.2 V versus SCE in CH_3CN. This result agrees with the photoanodic onset potential resolved from the CV curves in Figure 4 (∼ −0.3 V vs SCE). From the slope, N_D is estimated to be around 10^{15} cm^{-3} by taking ϵ as 25.9.[29] According to Figure 5, frequency dispersions[30] appear to exist. Surface-state manipulation and interference from the host are possible causes. Since control experiments show that the capacitance corresponding to bare NaY is greater than the space-charge capacitance of NaY|PbO_x, the host effect is thus negligible and the values of E_{fb} and N_D are considered to be reliable. Calculations based on the determined E_{fb} value predict that the valence-band edge (E_{VB}) of $PbO_{2(NaY)}$ is 0.9 ± 0.2 V versus SCE. Here, we assume that $E_{fb} \approx E_{CB}$ for most n-type semiconductors and that the band-gap energy (E_g) of $PbO_{x(NaY)}$ is 1.4 eV (taken from PbO_2). If the estimation of E_{VB} is valid, a photoinduced electron transfer from *N*-aminophthalimide (anodic onset potential ≈0.75 V in CH_3CN, Figure 6, trace b) to $PbO_{x(NaY)}$, as proposed in Scheme 2, is possible. A photoinduced alkene aziridination may thus occur, as described in eqs 2−6.

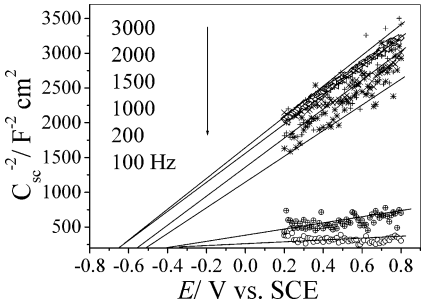

Figure 5. Typical Mott−Schottky plots for the NaY|PbO_x electrode in CH_3CN|0.1 M $TBAClO_4$. Frequency, 100−3000 Hz; perturbation signal, ±5 mV; scan rate, 5 mV s^{-1}.

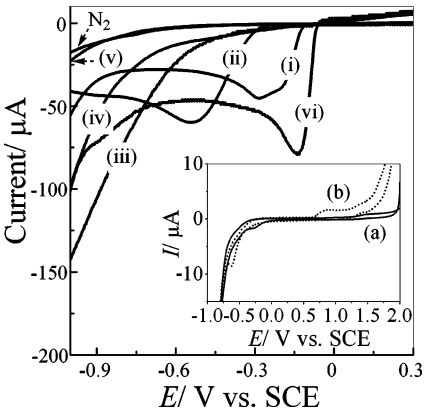

Figure 6. Typical LSV curves for the reduction of AgF (i), $AgNO_3$ (ii), $S_2O_8^{2-}$ (iii), H_2O_2 (iv), and O_2 (v) in CH_3CN. Trace vi: AgF under illumination. Inset: CV curves for the NaY|PbO_x electrode in CH_3CN|0.1 M $TBAClO_4$ in the absence (a) and in the presence (b) of 1 mM *N*-aminophthalimide.

For bulk photolysis, light harvesting is a crucial point. To increase the charge-separation lifetime and to prevent the undesired back reaction, that is, charge recombination, from happening, we employed AgF (i), $AgNO_3$ (ii), $S_2O_8^{2-}$ (iii), H_2O_2 (iv), and O_2 (v) as sacrificial acceptors (Figure 6). Silver fluoride appears to be the most promising candidate because its cathodic onset potential is the least negative, that is, ∼ −0.2 V versus SCE in the dark (trace i) and −0.15 V under illumination (trace vi). Unfortunately, AgF also caused undesirable photofluorination for reaction 1. $AgNO_3$ (onset potential ≈ −0.3 V; peak potential ≈ −0.5 V in CH_3CN) was thus taken as an alternative. According to the reaction profile shown in Figure 7 (inset), silver

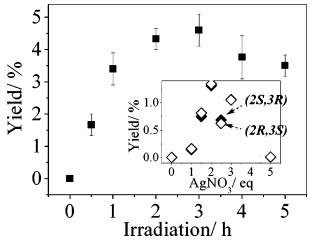

Figure 7. Reaction profiles in terms of total yields of (2*R*,3*S*)- and (2*S*,3*R*)-*N*-phthalimidoaziridine isomers vs photolysis period ([$AgNO_3$]: 2 equiv relative to *N*-aminophthalimide). The inset shows the yield vs [$AgNO_3$] in 25 mL of CH_3CN after a 1-h photolysis: [imide], 1 mM; [alkene], 1 mM; NaY|PbO_x, 40 mg.

SCHEME 2: Energetic Diagram for the $PbO_{x(NaY)}$-Sensitized Aziridination Reaction

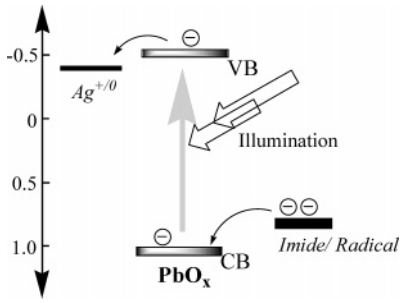

nitrate appears to be a qualified acceptor that can scavenge the electrons accumulated on the surface of NaY|PbO_x, as expected by the energetic diagram shown in Scheme 2. During illumination, metallic silver was formed and deposited on the surface of NaY|PbO_x. The formed metallic silver, from the electrochemical point of view, may work as a conductive component to facilitate charge transport on NaY|PbO_x. However, light blocking is also likely to occur in this case. Probably due to this or another reason, lower yields were observed with highly concentrated silver nitrate. A longer period of photolysis can improve the yield slightly. A period of 1 h seems to be sufficient for the typical reaction sensitized with 40 mg of NaY|PbO_x and 2 equiv of $AgNO_3$ (relative to imide).

For a successful photosensitization, most of the radiation should be absorbed within the space-charge region. In other words, the penetration depth of light must be compatible with the thickness of the space-charge layer (L):[31]

$$L = [2\epsilon\epsilon_0\Delta\phi/(eN_D)]^{1/2} \approx (1.1 \times 10^6\epsilon\Delta\phi/N_D)^{1/2} \quad \text{(in centimeters)} \quad (9)$$

According to eq 9, an L value of 2×10^{-5} to 1×10^{-4} cm (in the case of $N_D \approx 10^{15}$ cm^{-3}) may result if a band bending ($\Delta\phi$) of 10 mV−0.5 V is formed as $PbO_{x(NaY)}$ is in contact with electrolytes. On the assumption that the absorption of light by $PbO_{x(NaY)}$ follows a Beer's law relationship with an absorption coefficient of α (for semiconductors, $\alpha \leq 10^5$ cm^{-1}), the penetration depth of light (taken as $1/\alpha$) is calculated to be around 10^{-5} cm. Comparison of L with $1/\alpha$ implies that light may not be able to penetrate the depletion layer of $PbO_{x(NaY)}$ sufficiently far to excite the majority carriers. The quantum efficiency of NaY|PbO_x may thus be restricted to a less significant value. This drawback explains why when we varied the doping density for NaY|PbO_x by annealing the zeolite with hydrogen at 800 °C, the yield for reaction 1 revealed a relationship with N_D like that shown in Figure 8, slightly increasing with an increase in N_D. Nevertheless, charge leakage

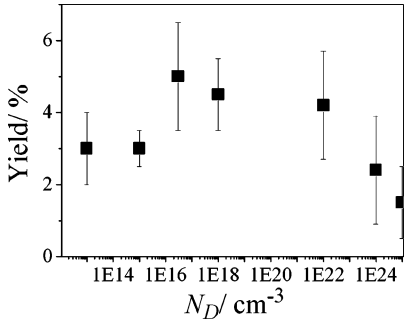

Figure 8. Relationship between the total yields of (2*R*,3*S*)- and (2*S*,3*R*)-*N*-phthalimidoaziridines and N_D in NaY|PbO_x.

TABLE 1: Impacts of Photocatalysts and Their Energetics (E_{VB} or $E^{o\prime}$*)

catalyst	E*/V vs SCE	HPLC yield/%
NaY|PbO_x	0.9[a]	3
PbO_x (polycrystalline)	0.9[b]	1
n-TiO_2 (rutile)	~2.0[c]	5
n-TiO_2 (anatase)	~2.0	5
clay|AcH^+	2.0[d]	<1
CdS	1.4[e]	<1
NaY|CA	1.2[f]	<1
NaY|$Ru(bpy)_3^{2+}$	~0.8[g]	<1
NaY		≪1

[a] This work. [b] Reference 26. [c] Reference 33a. [d] Reference 11. [e] Reference 34. [f] Reference 15. [g] Reference 35.

may occur if L gets thinner with an increase in N_D. Likely due to this effect, low yields were also observed when $PbO_{x(NaY)}$ was heavily doped ($N_D \gg 10^{24}$ cm^{-3}).

Several other photocatalysts (equal weight, 40 mg) were also tested for comparison. Table 1 lists their catalytic impacts and the energetics as they are brought to their excited states (E_{VB} or $E^{o\prime}$*). n-Type TiO_2 (anatase or rutile) appears to be the most effective catalyst. We consider this to be reasonable because the valence-band edge of TiO_2 can reach 3 V versus a normal hydrogen electrode (NHE) at pH 0 or 2 V versus SCE in aprotic media.[32] A wide variety of organic molecules can thus be photooxidized by TiO_2.[33] Nevertheless, TiO_2 produced significant amounts of side products besides the aziridine isomers. The selectivity for the aziridine isomers was <50% in this case. The other photosensitizers, such as cadmium sulfide (CdS),[34] cyanoanthracene (CA),[15] and $Ru(bpy)_3^{2+}$,[35] with similar energetics to those of $PbO_{x(NaY)}$, produced lower yields than NaY|PbO_x under similar conditions. Polycrystalline PbO_x (in equal weight) did not produce greater yields for reaction 1 either. This result highlights that NaY may provide a greater cross section for PbO_x or that the negatively charged framework of zeolite can effectively stabilize the imide cation derived in reaction 4. Likely due to these reasons, NaY|PbO_x shows a greater catalytic effect than polycrystalline PbO_x on reaction 1. Taking into account the effects discussed above and the low effective concentration of PbO_x in NaY|PbO_x (<20 μg/g of NaY based on the XPS intensities), we conclude that the prepared $PbO_{x(NaY)}$ is a potential photocatalyst for reaction 1.

One of the ultimate goals in our current research is to develop a stereoselective transformation mechanism for asymmetric synthesis. Previously, we observed that incorporating appropriate camphor-derived chiral ligands with lead acetate could manipulate the ee value for reaction 1.[5] For instance, with 1 equiv of chiral ligand 1 (relative to *N*-aminophthalimide), a 67−95% ee could be harvested, varying with the alkene molecule incorporated. In contrast, chiral ligand 2 gave a less significant impact on this issue. Regarding this issue, we thought

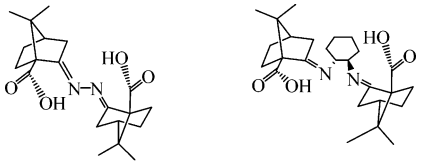

Chiral ligand 1 Chiral ligand 2

that chiral ligand 1 might strongly interact with Pb^{IV}, as proposed in eq 10. The chirality of chiral ligand 1 can thus influence the

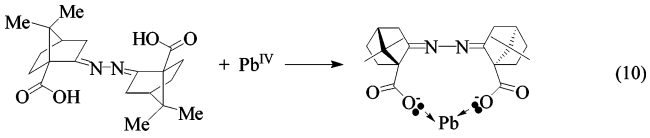

(10)

electron transfer between *N*-aminophthalimide and the electrochemical center, Pb^{IV}. In this work, we find that chiral ligand 1 also exhibits a similar effect on the photoaziridination reaction mediated by NaY|PbO_x. As shown in Figure 9, when 1.5 equiv of chiral ligand 1 (relative to the imide) is added into the system, as in Figure 7, the (2*R*,3*S*) isomer is produced with a higher yield, favoring this isomer with 30% ee. Regarding this effect, we carried out X-ray absorption spectral measurements for NaY|PbO_x. The Pb L_{III}-edge-structure spectra (XANES) recorded in the presence and in the absence of chiral ligands 1 and 2 are depicted in Figure 10; the derivative plots are shown in Figure 11 for comparison. Here, the *Y*-axis is taken from the first derivative of the intensity shown in Figure 10 with respect to energy. According to the derivative plots, the binding energy of Pb in NaY|PbO_x (curve b) is 13 035.96 eV, shifting by ~1 eV relative to Pb^0 determined from metallic lead (13 035 eV, curve a). Noticeably, when NaY|PbO_x is incorporated with chiral ligand 1, the Pb L_{III}-edge shifts to 13 038.574 eV ($\Delta \approx 2.6$ eV, curve c), whereas chiral ligand 2 only causes a slight shift ($\Delta < 0.1$ eV, curve d). The XANES is considered to be a direct probe of the oxidation state of the absorber atoms. It is basically agreed that a variation in oxidation state by ± 1 can cause a shift in binding energy by $\sim \pm 1.5$ eV. On the basis of this rule, chiral ligand 1 appears to behave like a bidentate agent to interact with $PbO_{x(NaY)}$, as proposed in eq 10. Because of this interaction, the chirality of chiral ligand 1 allows *N*-aminophthalimide to approach $PbO_{x(NaY)}$ in a restricted pathway. An asymmetric oxidation of *N*-aminophthalimide on the surface of the illuminated $PbO_{x(NaY)}$ thus occurs.

From the theoretical point of view, the coordination numbers found with the XANES and extended X-ray absorption fine-structure (EXAFS) techniques are averages over the absorber element atoms. Since some PbO_x is likely to be deeply trapped in the host, the binding-energy shift of Pb by chiral ligand 1 is thus smaller than 3 eV. From the point of view of bond strength, coordination bonds are somewhat weaker than covalent bonds. This is considered as another reason. Regarding the interaction between the chiral ligand and $PbO_{x(NaY)}$, XPS gave less information. This is likely due to the fact that only the lead oxide near or on the surface of the zeolite can virtually interact with the chiral ligands. Therefore, the XPS reflected from the bulk $PbO_{x(NaY)}$ remains less perturbed when chiral ligands are incorporated.

Regarding the binding energies of Pb species, Izumi et al. reported that the L_{III} edge of Pb^{II} in NaY is around 13 043 eV on the basis of the Pb $L\alpha_1$ emission spectra.[36] The binding energy of Pb in $PbO_{x(NaY)}$ is not available in this report. Comparing the data of Izumi et al. with ours on some other lead species, we consider that their data seem to be overenergetic

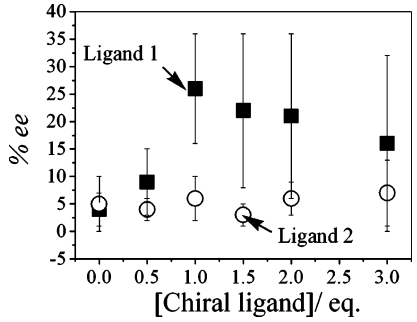

Figure 9. Relationships between % ee and the concentrations of chiral ligands (relative to *N*-aminophthalimide).

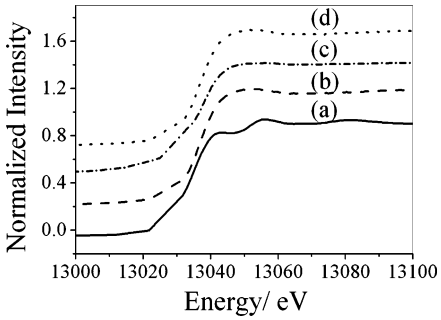

Figure 10. XANES spectra for metallic lead (a), NaY|PbO_x (b), NaY|PbO_x with chiral ligand 1 (c), and NaY|PbO_x with chiral ligand 2 (d).

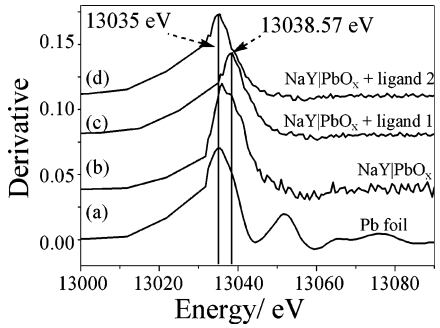

Figure 11. Derivative plots for metallic lead and NaY|PbO_x in the absence and in the presence of chiral ligands 1 and 2.

by ~5.6 eV. One possible cause is the low concentration of Pb^{II} in the samples. The other is the calibration of Pb^0 (13 040.6 eV). According to our data shown in Figure 11 (curve a), the binding energy of Pb^0 is around 13 035 eV, which is in good agreement with the values reported by Bearden et al. (13 035.2 eV).[37] Despite these, the XANES spectra depicted in Figures 10 and 11 have provided evidence showing that chiral ligand 1 can interact with $PbO_{x(NaY)}$ with a stronger affinity over chiral ligand 2. Because of this strong interaction, an asymmetric environment is created for *N*-aminophthalimide on the surface of $PbO_{x(NaY)}$. A preferential formation for the (2*S*,3*R*)-aziridine isomer becomes possible. Regarding the superiority of chiral ligand 1 over chiral ligand 2 in interacting with $PbO_{x(NaY)}$, a spacer with less steric hindrance between the two carboxylates, as shown in eq 10, is believed to play a crucial role.

Acknowledgment. The authors thank the National Science Council, Republic of China (NSC 92-2113-M-003-022) for financial support. Our gratitude also goes to the Academic Paper Editing Clinic, NTNU.

Supporting Information Available: Figures showing diffuse-reflectance absorption spectra for NaY, NaY|Pb^{2+}, and

$NaY|Pb^{2+}$ and XPS spectra of standard $Pb(NO_3)_2$ and PbO_x specimens. This material is available free of charge via the Internet at http://pubs.acs.org.

References and Notes

(1) (a) Kise, N.; Ozaki, H.; Moriyama, N.; Kitagishi, Y.; Ueda, N. *J. Am. Chem. Soc.* **2003**, *125*, 11591. (b) Córdova, A. *Acc. Chem. Res.* **2004**, *37*, 102.

(2) (a) Josephsohn, N. S.; Kuntz, K. W.; Snapper, M. L.; Hoveyda, A. H. *J. Am. Chem. Soc.* **2001**, *123*, 11594. (b) Pointillart, F.; Train, C.; Gruselle, M.; Villain, F.; Schmalle, H. W.; Talbot, D.; Gredin, P.; Decurtins, S.; Verdaguer, M. *Chem. Mater.* **2004**, *16*, 832. (c) Ojima, I. *Catalytic Asymmetric Synthesis II*; Wiley-VCH: New York, 2000.

(3) Tanner, D. *Angew. Chem., Int. Ed. Engl.* **1994**, *33*, 599.

(4) (a) Brandt, P.; Sodergren, M. J.; Andersson, P. G.; Norrby, P.-O. *J. Am. Chem. Soc.* **2000**, *122*, 8013. (b) Noda, K.; Hosoya, N.; Irie, R.; Ito, Y.; Katsuki, T. *Synlett* **1993**, 469. (c) Nishikori, H.; Katsuki, T. *Tetrahedron Lett.* **1996**, *37*, 9245. (d) Lai, T.-S.; Kwong, H.-L.; Che, C.-M.; Peng, S.-M. *Chem. Commun.* **1997**, 2373. (e) Au, S.-M.; Fung, W.-H.; Cheng, M.-C.; Che, C.-M.; Peng, S.-M. *Chem. Commun.* **1997**, 1655. (f) Müller, P.; Baud, C.; Jacquier, Y. *Can. J. Chem.* **1998**, *76*, 738. (g) Evans, D. A.; Faul, M. M.; Bilodeau, M. T. *J. Org. Chem.* **1991**, *56*, 6744. (h) Evans, D. A.; Faul, M. M.; Bilodeau, M. T.; Anderson, B. A.; Barnes, D. M. *J. Am. Chem. Soc.* **1993**, *115*, 5328. (i) Evans, D. A.; Faul, M. M.; Bilodeau, M. T. *J. Am. Chem. Soc.* **1994**, *116*, 2742. (j) Li, Z.; Conser, K. R.; Jacobsen, E. J. *J. Am. Chem. Soc.* **1993**, *115*, 5326. (k) Li, Z.; Quan, R. W.; Jacobsen, E. J. *J. Am. Chem. Soc.* **1995**, *117*, 5889.

(5) (a) Yang, K. S.; Chen, K. *Org. Lett.* **2002**, *4*, 1107. (b) Yang, K. S.; Chen, K. *J. Org. Chem.* **2001**, *66*, 1676.

(6) Anastas, P. T.; Kirchhoff, M. M. *Acc. Chem. Res.* **2002**, *35*, 686.

(7) Siu, T.; Yudin, A. K. *J. Am Chem. Soc.* **2002**, *124*, 530.

(8) (a) Hara, K.; Sayama, K.; Ohga, Y.; Shinpo, A.; Suga, S.; Arakawa, H. *Chem. Commun.* **2001**, 569. (b) Nazeeruddin, M. K.; Kay, A.; Rodicio, I.; Humphry-Baker, R.; Mueller, E.; Liska, P.; Vlachopoulos, N.; Graetzel, M. *J. Am. Chem. Soc.* **1993**, *115*, 6382.

(9) (a) Gust, D.; Moore, T. A.; Moore, A. L. *Acc. Chem. Res.* **2001**, *34*, 40. (b) Gust, D.; Moore, T. A. In *The Porphyrin Handbook*; Kadish, K. M., Smith, K. M., Guilard, R., Eds.; Academic Press: New York, 2000; pp 153−190. (c) Sakata, Y.; Imahori, H.; Sugiura, K.-I. *J. Inclusion Phenom. Macrocyclic Chem.* **2001**, *41*, 31.

(10) (a) Krueger, J. S.; Mayer, J. E.; Mallouk, T. E. *J. Am. Chem. Soc.* **1988**, *110*, 8232. (b) Kim, Y.; Mallouk, T. E. *J. Phys. Chem.* **1992**, *96*, 2789. (c) Borja, M.; Dutta, P. K. *Nature* **1993**, *362*, 43.

(11) Teng, Y.-W.; Chang, I.-J.; Wang, C. M. *J. Phys. Chem. B* **1997**, *101*, 10386.

(12) (a) Colon, J. L.; Yang, C. Y.; Clearfield, A.; Martin, C. R. *J. Phys. Chem.* **1990**, *94*, 874. (b) Thomas, J. K. *Chem. Rev.* **1993**, *93*, 301.

(13) (a) Torracca, E.; Galli, P.; Pansini, M.; Colella, C. *Microporous Mesoporous Mater.* **1998**, *20*, 119. (b) Langella, A.; Pansini, M.; Cappelletti, P.; de Gennaro, B.; de'Gennaro, M. *Microporous Mesoporous Mater.* **2000**, *37*, 337.

(14) (a) Baretz, B.; Turro, N. J. *J. Photochem.* **1984**, *24*, 201. (b) Iu, K. K.; Thomas, J. K. *Langmuir* **1990**, *6*, 471. (c) Liu, X.; Iu, K. K.; Thomas, J. K. *J. Phys. Chem.* **1989**, *93*, 4120. (d) Sarkar, N.; Das, K.; Natha, D. N.; Bhattacharyya, K. *Langmuir* **1994**, *10*, 326. (e) Zhang, G.; Kerry, T. J. *J. Phys. Chem. B* **2003**, *107*, 7254. (f) Yoon, K. B. *Chem. Rev.* **1993**, *93*, 321. (g) Murray, D.; Chang, J. W.; Haw, J. F. *J. Am. Chem. Soc.* **1993**, *115*, 4732. (h) Murray, D. K.; Howard, T.; Goguen, P. W.; Krawietz, T. R.; Haw, J. F. *J. Am. Chem. Soc.* **1994**, *116*, 6354.

(15) Chang, Y. C.; Chang, P. W.; Wang, C. M. *J. Phys. Chem. B* **2003**, *107*, 1628.

(16) Krueger, J. S.; Mallouk, T. E. In *Kinetics and Catalysis in Microheterogeneous Systems*; Grätzel, M., Kalyanasundaram, K., Eds.; Marcel Dekker: New York, 1991; Chapter 13.

(17) Chang, J. S.; Liu, L. K.; Wang, C. M. *Jpn. J. Appl. Phys.* **1996**, Part 2, *35*, L1402.

(18) (a) Grant, C. D.; Schwartzberg, A. M.; Smestad, G. P.; Kowalik, J.; Tolbert, L. M.; Zhang, J. Z. *J. Electroanal. Chem.* **2002**, *522*, 40. (b) Dürr, H.; Bouas-Laurent, H. *Photochromism, Molecules and Systems*; Elsevier: Amsterdam, The Netherlands, 1990.

(19) (a) Grätzel, M.; O'Regan, B. *Nature* **1991**, *353*, 737. (b) Fujishima, A.; Honda, K. *Nature* **1972**, *238*, 37.

(20) Yao, J. N.; Hashimoto, K.; Fujishima, A. *Nature* **1992**, *355*, 624.

(21) Bechinger, C.; Ferrere, S.; Zaban, A.; Sprague, J.; Gregg, B. A. *Nature* **1996**, *383*, 608.

(22) (a) Pavlov, D.; Zanova, S.; Papazov, G. *J. Electrochem. Soc.* **1977**, *124*, 1522. (b) Matsumoto, Y.; Noguchi, M.; Matsunaga, T. *J. Phys. Chem. B* **1999**, *103*, 7190. (c) Vigneron, J.; Redon, A. M.; Heindl, R.; Martin, J. C.; Sella, C. *Solar Cells* **1981**, *5*, 25. (d) Davidson, R. S.; Willsher, C. J. *J. Appl. Electrochem.* **1982**, *12*, 517. (e) Tremer, S. E.; Feng, J.; Johnson, D. C. *J. Electrochem. Soc.* **2001**, *148*, E321. (f) Montaser, A. A.; Veluchamy, P.; Minoura, H. *J. Electroanal. Chem.* **1996**, *419*, 47.

(23) Kumar, A.; Henglein, A.; Weller, H. *J. Phys. Chem.* **1989**, *93*, 2262.

(24) Moulder, J. F.; Stickle, W. F.; Sobol, P. E.; Bomben, K. D. In *Handbook of X-ray Photoelectron Spectroscopy: A Reference Book of Standard Spectra for Identification and Interpretation of XPS Data*; Chastain, J., Ed.; Perkin-Elmer Corporation, Physical Electronics Division: Eden Prairie, Mn, 1992; see also references therein.

(25) Buchanan, J. S.; Peter, L. M. *Electrochim. Acta* **1988**, *33*, 127.

(26) Hardee, K. L.; Bard, A. J. *J. Electrochem. Soc.* **1977**, *124*, 215.

(27) Schumacher, L. C.; Holzhueter, I. B.; Dignam, M. J. *J. Electroanal. Chem. Interfacial Electrochem.* **1989**, *261*, 331.

(28) Bard, A. J., Faulkner, L. R., Eds. *Electrochemical Methods: Fundamentals and Applications*, 2nd ed.; Wiley: New York, 2001; p 751.

(29) Lide, D. R., Ed. *Handbook of Chemistry and Physics*, 71st ed.; CRC Press: Boston, MA, 1990−1991; pp 12−26.

(30) Dutoit, E. C.; Van Menhaeghe, R. L.; Cardon, F.; Gomes, W. P. *Ber. Bunsen-Ges. Phys. Chem.* **1975**, *79*, 1206.

(31) Gerischer, H. In *Physical Chemistry: Advanced Treatise*; Eyring, H., Henderson, D., Jost, W., Eds.; Academic Press: New York, 1970; Vol. IXA, p 463.

(32) Wang, C. M.; Mallouk, T. E. *J. Phys. Chem.* **1990**, *94*, 4276.

(33) (a) Wang, C. M.; Mallouk, T. E. *J. Am. Chem. Soc.* **1990**, *112*, 2016. (b) Fox, M. A. *Acc. Chem. Res.* **1983**, *16*, 314. (c) Moser, J.; Graetzel, M. *J. Am. Chem. Soc.* **1983**, *105*, 6547.

(34) Darwent, J. R.; Porter, G. *Chem. Commun.* **1981**, 145.

(35) Kim, Y. I.; Mallouk, T. E. *J. Phys. Chem.* **1992**, *96*, 2879.

(36) Izumi, Y.; Kiyotaki, F.; Minato, T.; Seida, Y. *Anal. Chem.* **2002**, *74*, 3819.

(37) Bearden, J. A.; Burr, A. F. *Rev. Mod. Phys.* **1967**, *39*, 125.